Numerical Heat Transfer, Part A, 39:511–530, 2001

1040-7782/01 $12.00 + .00

COUPLED HEAT AND MASS TRANSFER BY NATURAL CONVECTION ABOUT A TRUNCATED CONE IN THE PRESENCE OF MAGNETIC FIELD AND RADIATION EFFECTS

Ali J. Chamkha
Department of Mechanical and Industrial Engineering, Kuwait University, Safat, 13060 Kuwait

This work is focused on steady, laminar, coupled heat and mass transfer by natural convective boundary layer flow over a permeable isothermal truncated cone in the presence of magnetic field and radiation effects. A suitable set of dimensionless variables is used and nonsimilar equations governing the problem are obtained. The resulting equations have the property that they reduce to various special cases previously considered in the literature. An adequate implicit, tridiagonal finite difference scheme is employed for the numerical solution of the obtained equations. Various comparisons with previously published work are performed and the results are found to be in excellent agreement. Representative results for the velocity, temperature, and concentration profiles as well as the local skin-friction coefficient; local Nusselt number and the local Sherwood number illustrating the influence of the Hartmann number; the concentration to thermal buoyancy ratio; and the wall mass transfer coefficient are presented and discussed.

INTRODUCTION

This article deals with steady, laminar, heat and mass transfer by natural convection hydromagnetic boundary layer flow around an isothermal permeable truncated cone. This flow and heat transfer situation is of considerable interest because it can occur in many geothermal, geophysical, technological, and engineering applications such as nuclear reactors, migration of moisture through air contained in fibrous insulations, grain storage, nuclear waste disposal, dispersion of chemical pollutants through water-saturated soil, and others. The geothermal gases are electrically conducting and are affected by the presence of a magnetic field. The same is found regarding the cooling of nuclear reactors (see Aldoss et al. [1]).

The natural convection heat transfer mode in various geometries has received a great deal of attention. For example, Kao [2] has reported on the local nonsimilarity solution for laminar natural convection adjacent to a vertical surface. Na [3] has considered natural convective flow past a nonisothermal vertical flat plate and reported a numerical solution. Lin and Chen [4] have studied mixed convection on a vertical plate for fluids on any Prandtl number. The laminar natural convection

Received 3 March 2000; accepted 1 November 2000.
Address correspondence to Ali J. Chamkha, Department of Mechanical and Industrial Engineering, Kuwait University, P.O. Box 596, Safat 13060, Kuwait

NOMENCLATURE

a_r	Rosseland mean extinction coefficient	U_r	reference velocity, $[g\cos\gamma\beta_T(T_w - T_\infty)x^*]^{1/2}$
B_o	magnetic induction	v	velocity component in the y-direction
c_p	specific heat at constant pressure	v_o	wall suction or injection velocity
C_f	local skin-friction coefficient, $2\upsilon(\partial u/\partial y)_{y=0}/U_r^2$	x	streamwise coordinate
D	mass diffusivity	x_o	distance of the leading edge of truncated cone measured from the origin
f	dimensionless stream function		
f_o	wall mass transfer coefficient, $v_o/\upsilon(x_o^4/\mathrm{Gr}_{xo})^{1/4}$	x^*	distance measured from the leading edge of the truncated cone, $x - x_o$
g	gravitational acceleration		
Gr_{x_*}	local Grashof number, $g\cos\gamma\beta_T(T_w - T_\infty)(x^*)^3/\upsilon^2$	y	transverse coordinate
h	local heat transfer coefficient	α	thermal diffusivity
h_m	local mass transfer coefficient	β_c	coefficient of concentration expansion
k	thermal conductivity		
M	Hartmann number, $(\sigma^* B_o^2/(\rho\upsilon)(x_o^4/\mathrm{Gr}_{x_o})^{1/2})^{1/2}$	β_T	coefficient of thermal expansion
		γ	half angle of the truncated cone
N	concentration to thermal buoyancy ratio, $\beta_c(c_w - c_\infty)/(\beta_T(T_w - T_\infty))$	η	pseudosimilarity variable
		ϕ	dimensionless concentration, $(c - c_\infty)/(c_w - c_\infty)$
Nu_{x^*}	local Nusselt number, hx^*/k	θ	dimensionless temperature, $(T - T_\infty)/(T_w - T_\infty)$
Pr	Prandtl number, υ/α		
r	local radius of the truncated cone	ξ	dimensionless distance
		υ	kinematic viscosity
r_t	surface temperature parameter, T_w/T_∞	ρ	density
		σ	Stefan–Boltzmann constant
R_d	radiation-conduction parameter, $4\sigma T_\infty^3/[k(a_r + \sigma_s)]$	σ^*	electrical conductivity
		σ_s	scattering coefficient
Sc	Schmidt number, υ/D	ψ	stream function
Sh_{x^*}	local Sherwood number, $h_m x^*/d$	**Subscripts**	
T	temperature	w	condition at the wall
u	velocity component in the x-direction	∞	condition at infinity

from a nonisothermal cone was analyzed by Hering and Grosh [5] and Roy [6]. An approximate method of solution for the overall heat transfer from vertical cones in laminar natural convection was reported by Alamgir [7]. The laminar natural convection over a slender vertical frustum of a cone has been studied by Na and Chiou [8, 9].

Hydromagnetic and thermal radiation effects also have been considered extensively in the literature. For example, Kafoussias [10] has analyzed hydromagnetic free convection flow through a nonhomogeneous porous medium over an isothermal cone surface. Kumari et al. [11] have considered nonaxisymmetric unsteady motion over a rotating disk in the presence of natural convection and magnetic field effects. Raptis and Singh [12] have solved the problem of hydromagnetic natural convection flow past an accelerated vertical plate. Takhar and Ram [13] have studied

magnetohydrodynamic natural convection flow of water through a porous medium. Thermal radiation effects become important when the difference between the surface and the ambient temperature is large. Viskanta and Grosh [14] have considered boundary layer flow in thermal radiation absorbing and emitting media. Ali et al. [15] have considered natural convection-radiation interaction in boundary layer flow over horizontal surfaces. Hossain and coworkers [16–18] have reported on natural convection radiation interaction from an inclined plate and vertical cylinders with circular elliptic cross sections.

Recently, Yih [19] reported on the effects of radiation on natural convection about a truncated cone. He obtained nonsimilar equations using a suitable transformation that were solved by the Keller box method. The purpose of this work is to generalize the work of Yih [19] through the inclusion of mass diffusion effects, hydromagnetic effects, and wall suction or injection effects.

GOVERNING EQUATIONS

Consider steady, laminar, heat and mass transfer by natural convection, boundary layer flow of an electrically conducting and optically dense fluid about a truncated permeable cone with a half angle γ in the presence of thermal radiation effects as shown in Figure 1. The origin of the coordinate system is placed at the vertex of the full cone where x represents the distance along the cone and y represents the distance normal to the surface of the cone. The cone surface is maintained at a constant temperature T_w and a constant concentration c_w, and the ambient temperature and concentration far away from the surface of the cone T_∞ and c_∞ are assumed to be uniform. For $T_w > T_\infty$ and $c_w > c_\infty$ an upward flow is induced as a result of the thermal and concentration buoyancy effects. Fluid suction or injection is imposed at the surface. A uniform magnetic field is applied in the y-direction normal to the flow direction. The magnetic Reynolds number is assumed to be small so that the induced magnetic field is neglected. In addition, the Hall effect and the electric field are assumed negligible. The small magnetic Reynolds number assumption uncouples the Navier–Stokes equations from Maxwell's equations. All physical properties are assumed constant except the density in the buoyancy force term. By inovoking all of the boundary layer. Boussineq, and Rosseland diffusion approximations (see, for instance, Yih [19]) the governing equations for this investigation can be written as

$$\frac{\partial(ru)}{\partial x} + \frac{\partial(rv)}{\partial y} = 0 \tag{1}$$

$$u\frac{\partial u}{\partial x} + v\frac{\partial u}{\partial y} = \upsilon\frac{\partial^2 u}{\partial y^2} + g\beta_T(T - T_\infty)\cos\gamma + g\beta_c(c - c_\infty)\cos\gamma - \frac{\sigma^* B_o^2}{\rho}u \tag{2}$$

$$u\frac{\partial T}{\partial x} + v\frac{\partial T}{\partial y} = \alpha\frac{\partial^2 T}{\partial y^2} + \frac{16\sigma}{3(a_r + \sigma_s)\rho c_p}\frac{\partial}{\partial y}\left(T^3\frac{\partial T}{\partial y}\right) \tag{3}$$

$$u\frac{\partial c}{\partial x} + v\frac{\partial c}{\partial y} = D\frac{\partial^2 c}{\partial y^2} \tag{4}$$

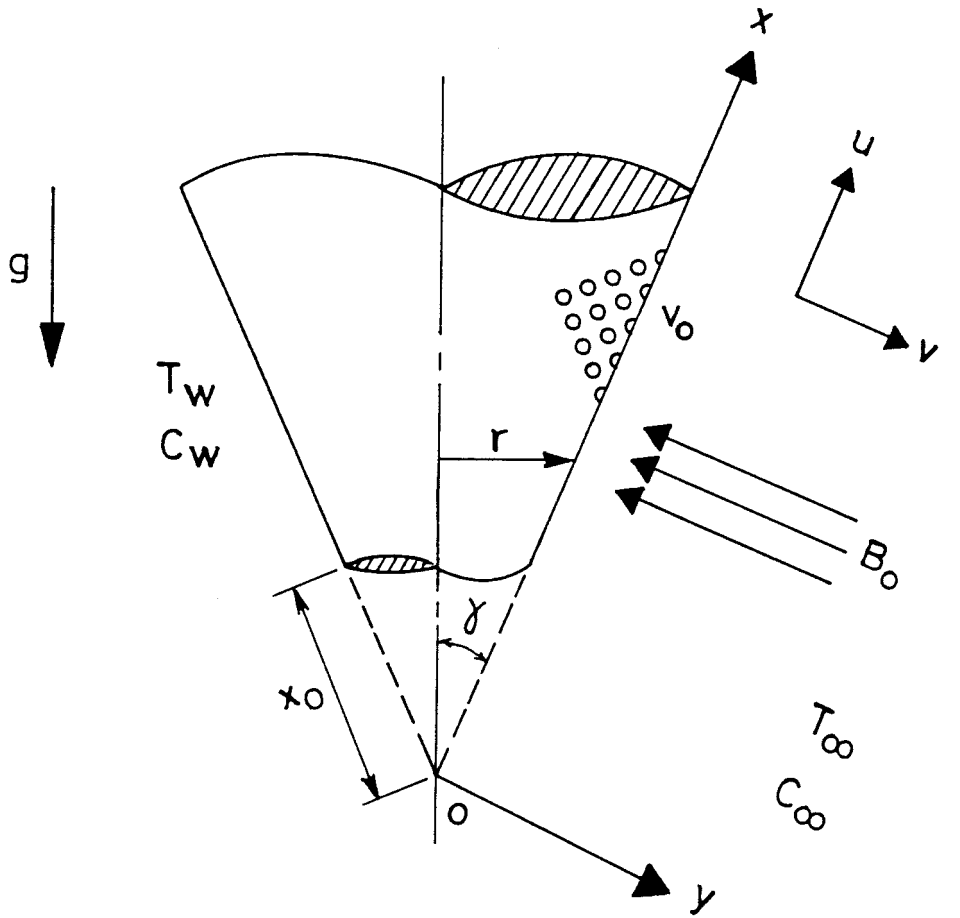

Figure 1. Problem schematics and coordinate system.

where r is the radius of the truncated cone. u, v, T, and c are the x-component of velocity, y-component of velocity, temperature, and concentration, respectively. ρ, υ, c_p, α, and D are the fluid density, kinematic viscosity, specific heat at constant pressure, thermal diffusivity, and mass diffusivity, respectively. σ^*, B_o, β_T, and β_c are the fluid electrical conductivity, magnetic induction, thermal expansion coefficient, and concentration expansion coefficient, respectively. g, σ, σ_s, and a_r are the acceleration due to gravity, Stefan–Boltzmann constant, scattering coefficient, and the Rosseland mean extinction coefficient, respectively. The coefficient of the last term of Eq. (3) is sometimes called radiative conductivity as mentioned by Yih [19].

The proper boundary and ambient conditions for this problem can be written as

$$y = 0: \quad u = 0 \quad v = -v_o \quad T = T_w \quad c = c_w \tag{5}$$

$$y \to \infty : \quad u \to 0 \quad T \to T_\infty \quad c \to c_\infty \tag{6}$$

where v_0 (> 0) is the wall suction velocity.

The governing equations and boundary conditions can be made dimensionless by introducing the stream function such that

$$ru = \frac{\partial \psi}{\partial y} \qquad rv = -\frac{\partial \psi}{\partial x} \tag{7}$$

and using the following dimensionless variables

$$\begin{aligned}
&\xi = \frac{x - x_o}{x_o} = \frac{x^*}{x_o} \quad \eta = \frac{y}{x^*}(\mathrm{Gr}_{x^*})^{1/4} \quad \mathrm{Gr}_{x^*} = g\beta_T(T_w - T_\infty)x^{*3}/\upsilon^2 \\
&f(\xi, \eta) = \frac{\psi}{r\upsilon(\mathrm{Gr}_{x^*})^{1/4}} \quad \theta(\xi, \eta) = \frac{T - T_\infty}{T_w - T_\infty} \quad \phi(\xi, \eta) = \frac{c - c_\infty}{c_w - c_\infty} \\
&u = \frac{\upsilon(\mathrm{Gr}_{x^*})^{1/2}}{x^*} f' = U_r f' \\
&v = -\frac{\upsilon(\mathrm{Gr}_{x^*})^{1/4}}{x^*}\left[\left(\frac{\xi}{1+\xi} + \frac{3}{4}\right) f + \xi \frac{\partial f}{\partial \xi} - \frac{1}{4}\eta f'\right]
\end{aligned} \tag{8}$$

where U_r is a reference velocity.

Substituting Eqs. (7) and (8) into Eqs. (1) thorough (6) yields the following nonsimilar dimensionless equations:

$$f''' + \left(\frac{\xi}{1+\xi} + \frac{3}{4}\right) f f'' - \frac{1}{2}(f')^2 - M^2 \xi^{1/2} f' + \theta + N\phi = \xi\left(f' \frac{\partial f'}{\partial \xi} - f'' \frac{\partial f}{\partial \xi}\right) \tag{9}$$

$$\frac{\theta''}{\mathrm{Pr}} + \left(\frac{\xi}{1+\xi} + \frac{3}{4}\right) f \theta' + \frac{4}{3}\frac{R_d}{\mathrm{Pr}}\{\theta'[(r_t - 1)\theta + 1]^3\}' = \xi\left(f' \frac{\partial \theta}{\partial \xi} - \theta' \frac{\partial f}{\partial \xi}\right) \tag{10}$$

$$\frac{\phi''}{\mathrm{Sc}} + \left(\frac{\xi}{1+\xi} + \frac{3}{4}\right) f \phi' = \xi\left(f' \frac{\partial \phi}{\partial \xi} - \phi' \frac{\partial f}{\partial \xi}\right) \tag{11}$$

$$\eta = 0 : \quad f' = 0 \quad f_o \xi^{1/4} = \left(\frac{\xi}{1+\xi} + \frac{3}{4}\right) f + \xi \frac{\partial f}{\partial \xi} \quad \theta = 1 \quad \phi = 1 \tag{12}$$

$$\eta \to \infty : \quad f' \to 0 \quad \theta \to 0 \quad \phi \to 0 \tag{13}$$

where a prime denotes partial differentiation with respect to η and

$$\begin{aligned}
&M^2 = \frac{\sigma B_o^2}{\rho \upsilon}\left(\frac{x_o^4}{\mathrm{Gr}_{x_o}}\right)^{1/2} \quad N = \frac{\beta_c(c_w - c_\infty)}{\beta_T(T_w - T_\infty)} \quad \mathrm{Pr} = \frac{\upsilon}{\alpha} \\
&R_d = \frac{4\sigma T_\infty^3}{[k(a_r + \sigma_s)]} \quad r_t = \frac{T_w}{T_\infty} \quad \mathrm{Sc} = \frac{\upsilon}{D} \quad f_o = \frac{v_o}{\upsilon}\left(\frac{x_o^4}{\mathrm{Gr}_{x_o}}\right)^{1/4}
\end{aligned} \tag{14}$$

are the square of the Hartmann number, concentration to thermal buoyancy ratio, Prandtl number, radiation-conduction parameter, surface temperature parameter, Schmidt number, and mass transfer coefficient, respectively. In these definitions,

$\mathrm{Gr}_{x_o} = g\beta_T(T_w - T_\infty)\cos\gamma x_o^3/\upsilon^2$ is the Grashof number based on x_o and k is the thermal conductivity.

Equations (9) through (11) represent general equations that include various special cases. For example, by formally setting all of f_o, M, N, and R_d equal to 0, Equations (9) and (10) reduce to those reported earlier by Na and Chiou [9] in their work concerning laminar natural convection over a frustum of a cone. Also, in the absence of magnetic field ($M = 0$), wall mass transfer effects ($f_o = 0$), and the concentration buoyancy effects ($N = 0$), Eqs. (9) and (10) reduce to those reported recently by Yih [19]. In addition, the similarity equations for flow and heat transfer by natural convection over a vertical plate reported previously by Na [3] are recovered by formally setting all of f_o, M, N, R_d, γ, and $\xi = 0$ in Eqs. (9) and (10). Furthermore, the similarity equations governing the flow and heat transfer about the full cone case (see, for instance, [5], [6], [7], and [9]) are obtained by taking $f_o = M = N = R_d = 0$ and letting $\xi \to \infty$.

The local skin-friction coefficient C_f, local Nusselt number Nu_{x*}, and the local Sherwood number Sh_{x*} are important physical properties. These can be defined in dimensionless form below as given by Yih [19]:

$$C_f = -2(\mathrm{Gr}_{x^*})^{-1/4} f''(\xi, 0) \quad \mathrm{Nu}_{x^*} = -\left(1 + \frac{4R_d r_l^3}{3}\right)(\mathrm{Gr}_{x^*})^{1/4}\theta'(\xi, 0)$$
$$\mathrm{Sh}_{x^*} = -(\mathrm{Gr}_{x^*})^{-1/4}\phi'(\xi, 0) \tag{15}$$

NUMERICAL METHOD

The initial value problem represented by Eqs. (9) through (13) with ξ playing the role of time is nonlinear and has no closed-form solution. Therefore, it must be solved numerically. The implicit, tridiagonal, finite difference method discussed by Blottner [20] has proven to be adequate for the accurate solution of boundary layer equations. For this reason, it is adopted in this work.

All first-order derivatives with respect to ξ are replaced by two-point backward difference quotients such that

$$\frac{\partial A}{\partial \xi} = \frac{A_{m,n} - A_{m-1,n}}{\Delta\xi_{m-1}} \tag{16}$$

where A is a typical independent variable, m and n indicate lines of constant ξ and constant η, respectively. $\Delta\xi_{m-1}$ is the ξ step size between the $m-1$ and m lines of constant ξ.

Equation (9) is converted into a second-order partial differential equation by letting $V = f'$. Then all equations governing V, θ, and ϕ can be written in the general form:

$$\pi_1 Z'' + \pi_2 Z' + \pi_3 Z + \pi_4 = 0 \tag{17}$$

where $Z = V$, θ, or ϕ and the π's are constants, functions of the dependent variables, or functions of the independent variables. These equations are discretized using three-point central difference quotients and, as a consequence, a set of algebraic equations results at each line of constant ξ. These algebraic equations are then solved by the well-known Thomas algorithm (see Blottner [20]) with iteration to deal with

the nonlinearities of the problem. When the solution at a specific line of constant ξ is obtained, the same solution procedure is used for the next line of constant ξ. This marching process continues until the desired value of ξ is reached. At each line of constant ξ, when V is known, the equation $f' = V$ is then solved for f using the trapezoidal rule. The convergence criterion employed was based on the difference between the current and the previous iterations. When this difference reached 10^{-5}, the solution was assumed converged and the iteration procedure was terminated. Variable step sizes in both the ξ and η directions were utilized to accommodate the sharp changes in the dependent variables especially in the immediate vicinity of the cone surface. The (ξ, η) computational domain consisted of 299 and 196 points, respectively. The initial step sizes in ξ and η were both taken to be equal to 10^{-3}, and the growth factors were taken to be 1.04 and 1.0375. This gave $\xi_\infty = 3000$ and $\eta_\infty = 35$. These values were found to give accurate grid-independent results as verified by the comparisons mentioned below.

To access the accuracy of the numerical results, various comparisons with previously published work for the cases of a vertical plate ($\xi = 0$) and a full cone ($\xi = \infty$) were performed. These comparisons are presented in Tables 1 and 2. It is obvious from these tables that excellent agreement between the results exists. These favorable comparisons lend confidence in the graphical results to be reported in the next section.

RESULTS AND DISCUSSION

In this section, a representative set of numerical results for the velocity, temperature, and concentration profiles as well as the local skin-friction coefficient, local Nusselt number, and the local Sherwood number is presented graphically in Figures 2 through 19. These results illustrate the effects of the Hartmann number M, the concentration to thermal buoyancy ratio N, and the suction or injection parameter f_o on the solutions.

Table 1. Comparison of values of $f''(0, 0)$ and $-\theta'(0, 0)$ for various values of Pr with $f_o = 0$, $M = 0$, $N = 0$, and $R_d = 0$

	$f''(0, 0)$			$-\theta'(0, 0)$						
Pr	[21]	[19]	Current results	[3]	[9]	[21]	[22]	[4]	[19]	Current results
0.0001	—	1.4998	1.4997	—	—	—	—	—	0.0060	0.0059
0.001	—	1.4728	1.4727	—	—	—	—	0.0187	0.0189	0.0188
0.01	—	1.3968	1.3965	0.0574	0.0574	—	0.057	0.0570	0.0570	0.0574
0.1	1.2104	1.2144	1.2151	—	—	0.1637	0.164	0.1627	0.1629	0.1630
1	0.9081	0.9084	0.9081	0.4010	0.4011	0.4009	0.401	0.4009	0.4012	0.4015
10	0.5930	0.5927	0.5927	0.8269	0.8269	0.8266	0.827	0.8258	0.8266	0.8274
100	0.3564	0.3559	0.3558	1.5493	1.5493	1.5495	1.550	1.5490	1.5493	1.5503
1000	—	0.2049	0.2049	—	—	—	2.800	2.8035	2.8035	2.8044
10,000	—	0.1161	0.1161	—	—	—	—	5.0125	5.0127	5.0131

Table 2 Comparison of values of $f''(\infty, 0)$ and $-\theta'(\infty, 0)$ for various values of Pr with $f_o = 0$, $M = 0$, $N = 0$, and $R_d = 0$

	$f''(\infty, 0)$				$-\theta'(\infty, 0)$					
Pr	[5]	[6]	[19]	Current results	[5]	[6]	[7]	[9]	[19]	Current results
0.0001	—	—	1.6006	1.6005	—	—	0.0071	—	0.0079	0.0078
0.001	1.5166	—	1.5135	1.5133	0.0247	—	0.0225	—	0.0246	0.0245
0.01	1.3550	—	1.3551	1.3549	0.0748	—	0.0709	0.0749	0.0749	0.0751
0.1	1.0960	—	1.0960	1.0962	0.2113	—	0.2141	—	0.2116	0.2116
1	0.7694	0.8600	0.7699	0.7697	0.5104	0.5275	0.5280	0.5104	0.5109	0.5111
10	—	0.4899	0.4877	0.4877	—	1.0354	1.0159	1.0340	1.0339	1.0342
100	—	0.2897	0.2896	0.2895	—	1.9229	1.8237	1.9220	1.9226	1.9230
1000	—	0.1661	0.1661	0.1661	—	3.4700	3.2463	—	3.4696	3.4700
10,000	—	0.0940	0.0940	0.0940	—	6.1998	5.7734	—	6.1984	6.1988

Figures 2 through 4 present typical profiles for the velocity along the cone f', temperature θ, and concentration ϕ for various values of the Hartmann number M, respectively. Application of a magnetic field normal to the flow of an electrically conducting fluid gives rise to a resistive force that acts in the direction opposite to that of the flow. This force is called the Lorentz force. This resistive force tends to slow down the motion of the fluid along the cone and causes increases in its temperature and concentration. This is depicted in Figures by the decreases in the values of f' and increases in the values of both θ and ϕ as M increases. These behaviors in f', θ, and ϕ are accompanied by increases in all of the hydrodynamic, thermal, and concentration boundary layers as M increases.

Figures 5 through 7 illustrate the effects of M on the local skin-friction coefficient C_f, local Nusselt number Nu_{x^*}, and the local Sherwood number Sh_{x^*}, respectively. As seen from the definitions of C_f, Nu_{x^*}, and Sh_{x^*}, they are directly proportional to $f''(\xi, 0)$, $-\theta'(\xi, 0)$, and $\phi'(\xi, 0)$, respectively. For this reason, they are shown in Figures 5 through 7. It was seen from Figures 2 through 4 that the wall slope of the velocity profile decreases while the slopes of both the temperature and concentration profiles increase as M increases. This produces reductions in all of C_f, Nu_{x^*}, and Sh_{x^*} as M increases as depicted in Figures 5 through 7. It is also observed from these figures that for $M > 0$ all of $f''(\xi, 0)$, $-\theta'(\xi, 0)$, and $-\phi'(\xi, 0)$ decrease with ξ while they increase with ξ for $M = 0$.

Figures 8 through 10 display the effects of the concentration to thermal buoyancy ratio N on the velocity, temperature, and concentration profiles, respectively. Positive values of N indicate aiding flow while negative values of N correspond to opposing flow. Increases in the values of N have a tendency to increase the buoyancy effects due to concentration difference. This induces more flow along the cone surface causing the velocity of the fluid to increase as evident from Figure 8. This increase in the flow velocity occurs at the expense of both the temperature and concentration, which decrease as N increases. It is interesting to note that the distinctive peaks in the velocity profiles move toward the cone surface as N

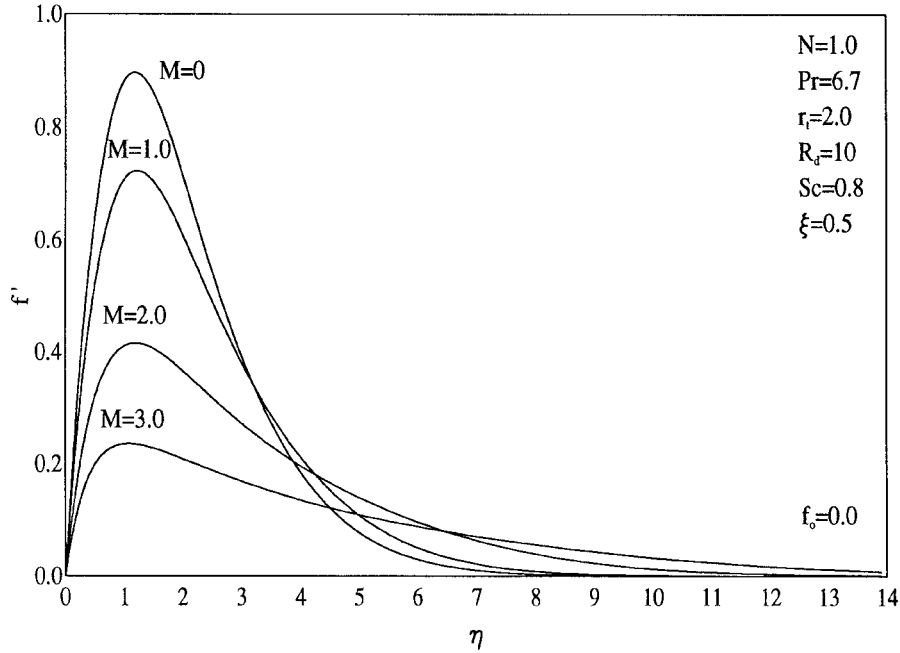

Figure 2. Effects of M on velocity profiles.

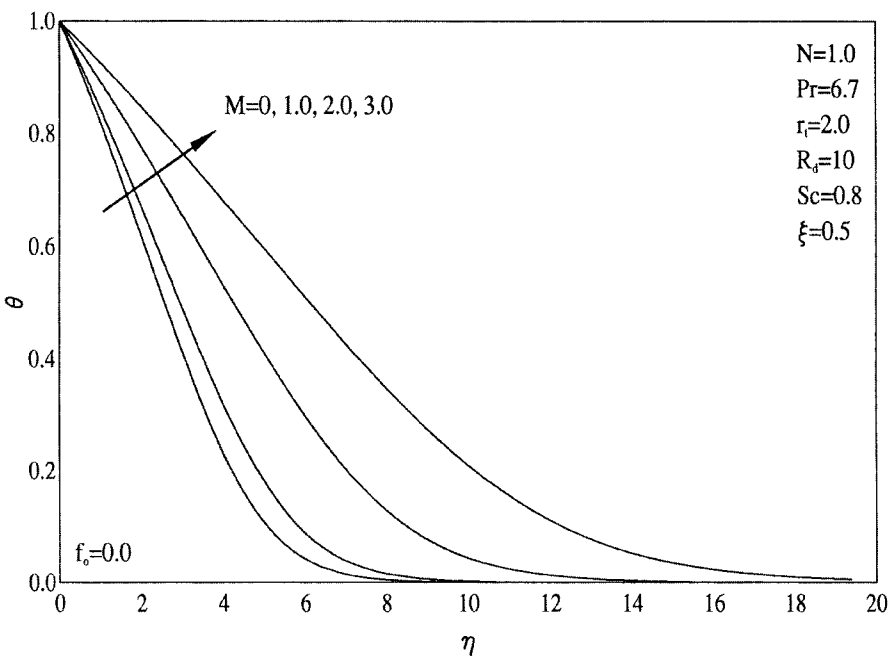

Figure 3. Effects of M on temperature profiles.

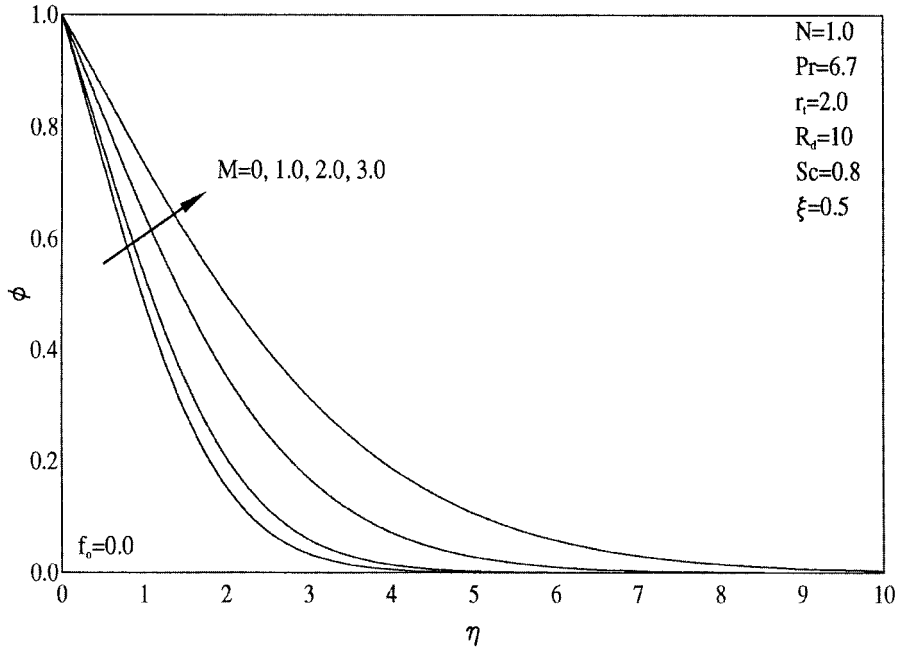

Figure 4. Effects of M on concentration profiles.

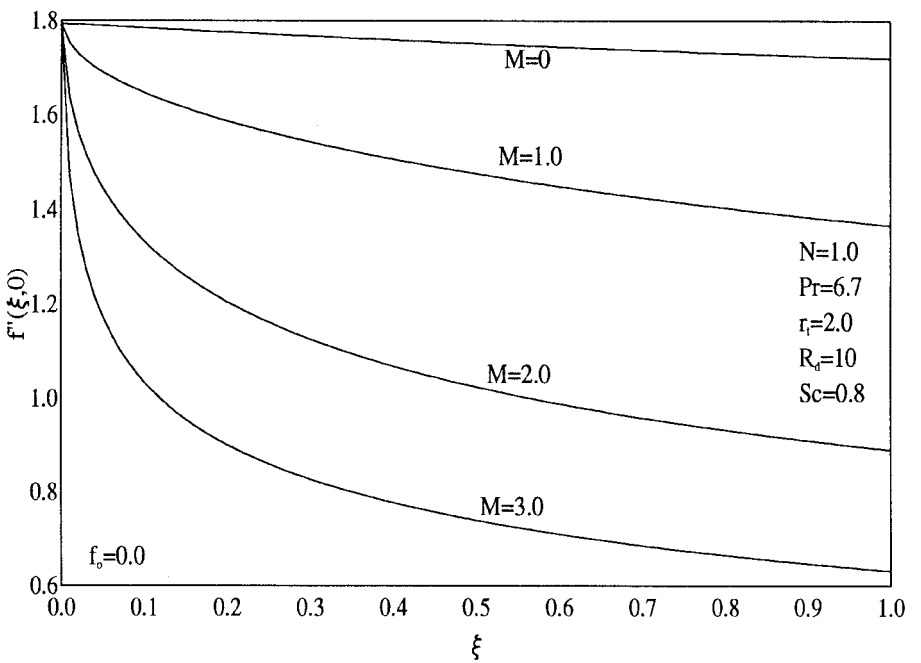

Figure 5. Effects of M on development of skin-friction coefficient.

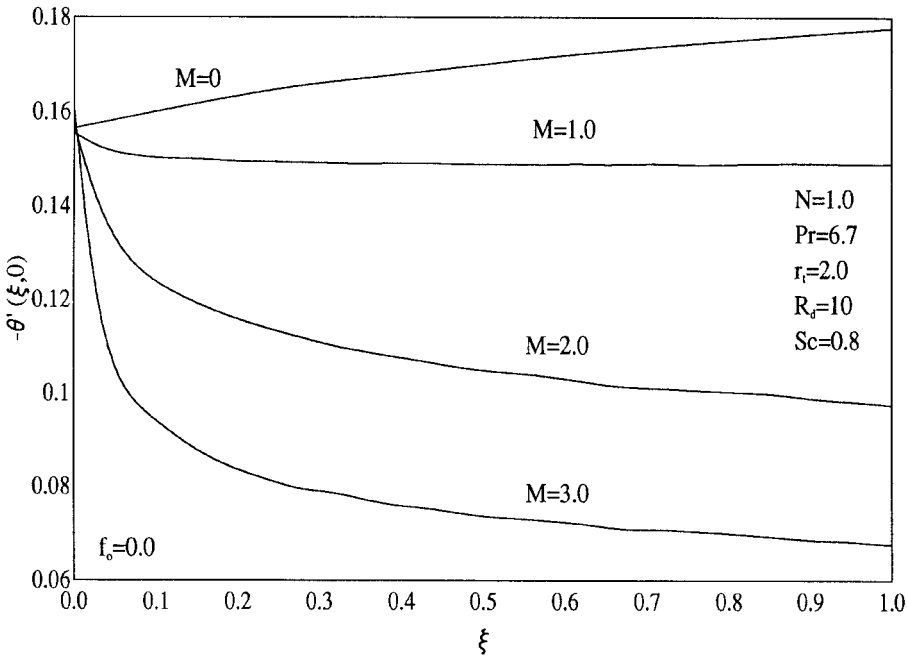

Figure 6. Effects of M on development of Nusselt number.

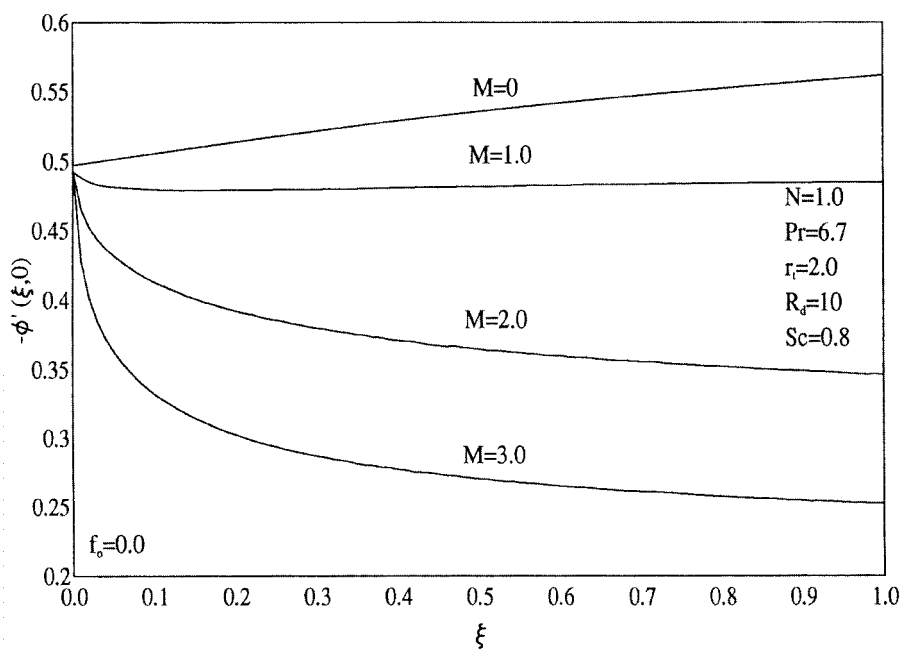

Figure 7. Effects of M on development of Sherwood number.

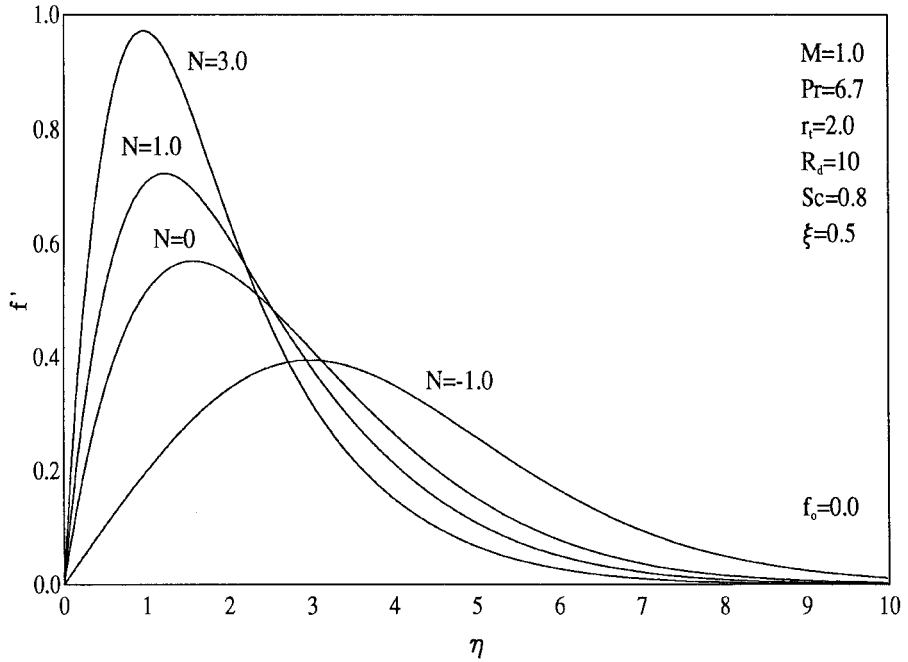

Figure 8. Effects of N on velocity profiles.

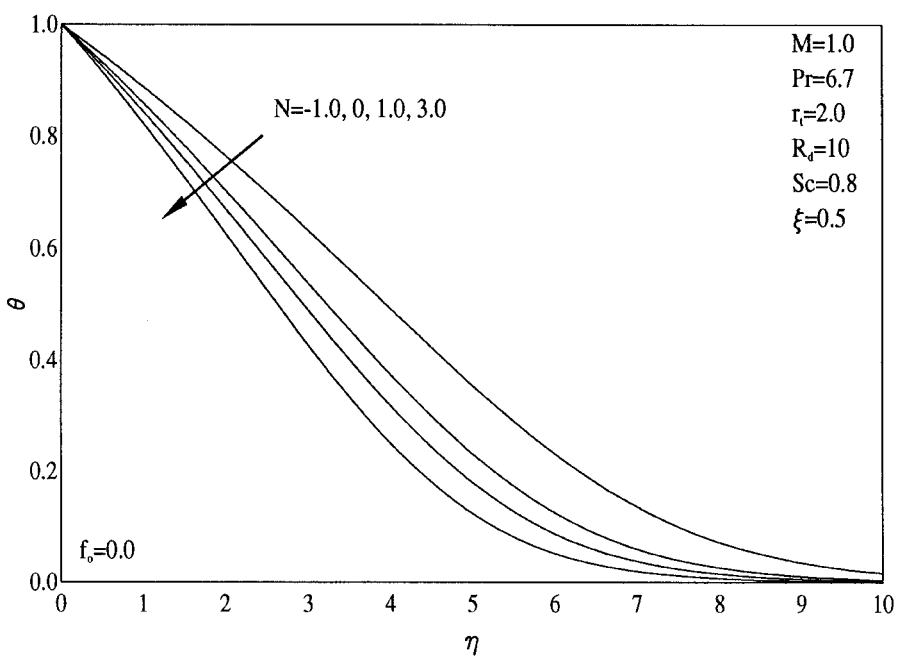

Figure 9. Effects of N on temperature profiles.

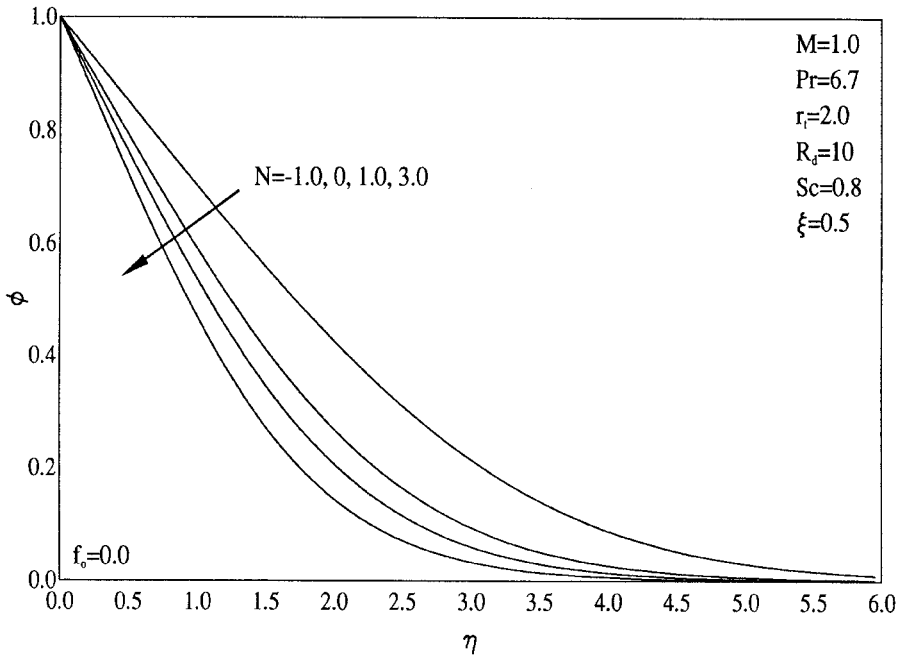

Figure 10. Effects of N on concentration profiles.

increases further and further. It is also observed that all of the hydrodynamic, thermal, and concentration boundary layers decrease as N increases.

Figures 11 through 13 depict the variations in the values of C_f (or $f''(\xi, 0)$), Nu_{x^*} (or $-\theta'(\xi, 0)$), and Sh_{x^*} (or $-\phi'(\xi, 0)$) as a result of changing the value of N, respectively. Inspection of Figures 8 through 10 shows that all of $f''(\xi, 0)$, $-\theta'(\xi, 0)$, and $-\phi'(\xi, 0)$ increase as N increases. This is true for all values of ξ as evident from Figures 11 and 13.

Figures 14 through 16 present representative velocity, temperature, and concentration profiles for various values of the wall mass transfer coefficient f_o and two values of the radiation-conduction parameter R_d, respectively. Imposition of fluid suction ($f_o > 0$) at the wall has a tendency to reduce all of the hydrodynamic, thermal, and concentration boundary layers. This causes all of the velocity, temperature, and concentration to decrease at every point far from the surface. On the other hand, injection of fluid ($f_o < 0$) through the surface produces the opposite effect, namely, increases in all of the velocity, temperature, and concentration. These behaviors are clearly shown in Figures 14 through 16. Consistent with the behavior reported by Yih [19], increasing the value of R_d results in increases in both the velocity and temperature distribution and the maximum velocity tends to move away from the surface. However, the concentration distribution tends to decrease as a result of increasing the radiation effect as observed from Figure 16.

The effects of both f_o and R_d on the development of the local skin-friction coefficient (or $f''(\xi, 0)$), the local Nusselt number (or $-\theta'(\xi, 0)$), and the local Sherwood number (or $-\phi'(\xi, 0)$) are displayed in Figures 17 through 19, respectively.

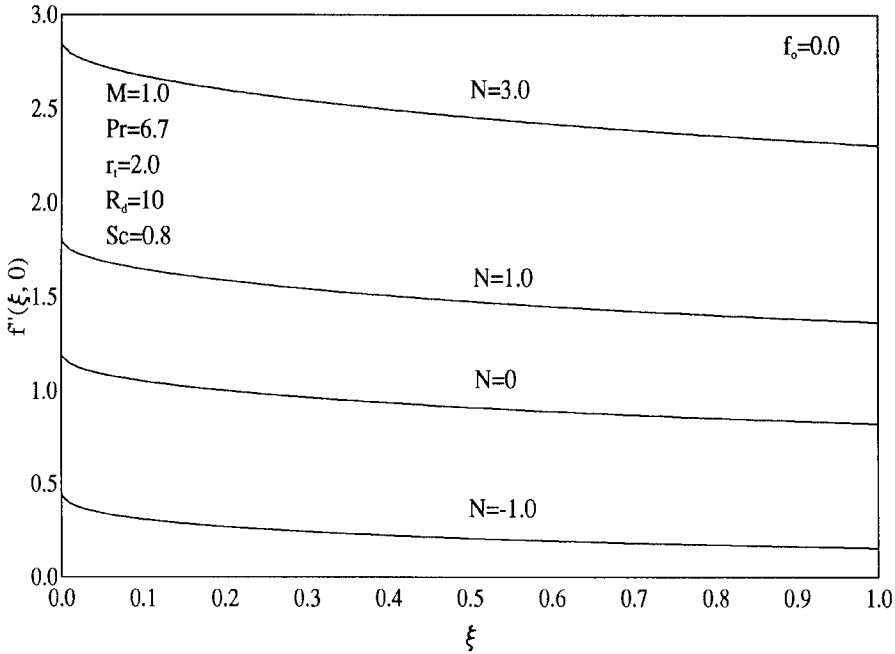

Figure 11. Effects of N on development of skin-friction coefficient.

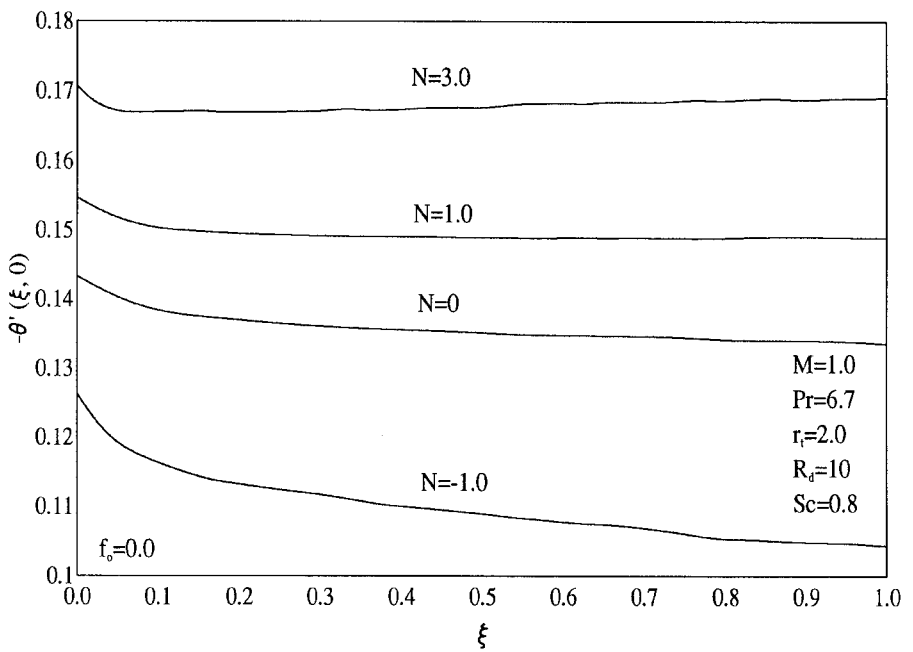

Figure 12. Effects of N on development of Nusselt number.

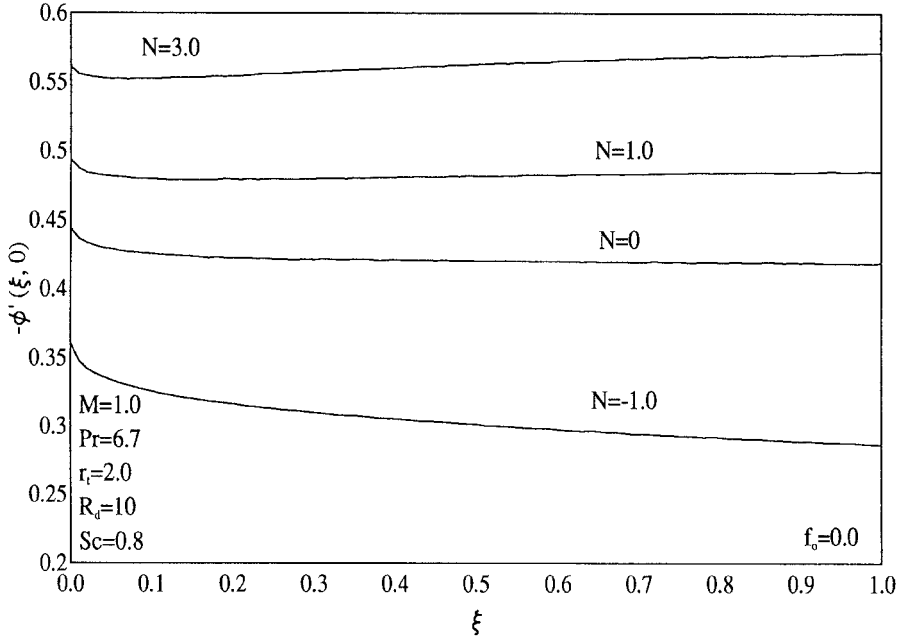

Figure 13. Effects of N on development of Sherwood number.

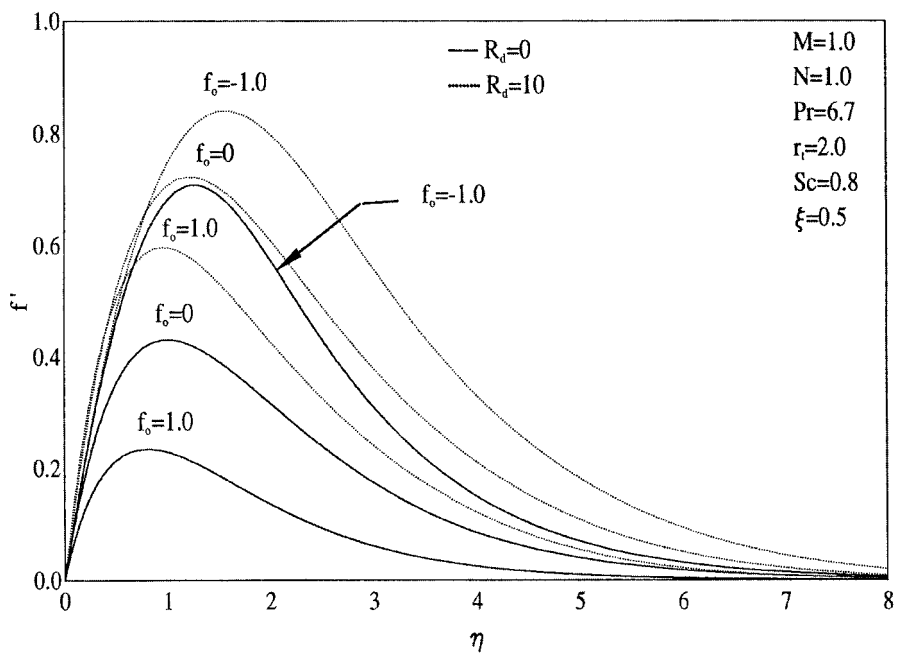

Figure 14. Effects of f_o and R_d on velocity profiles.

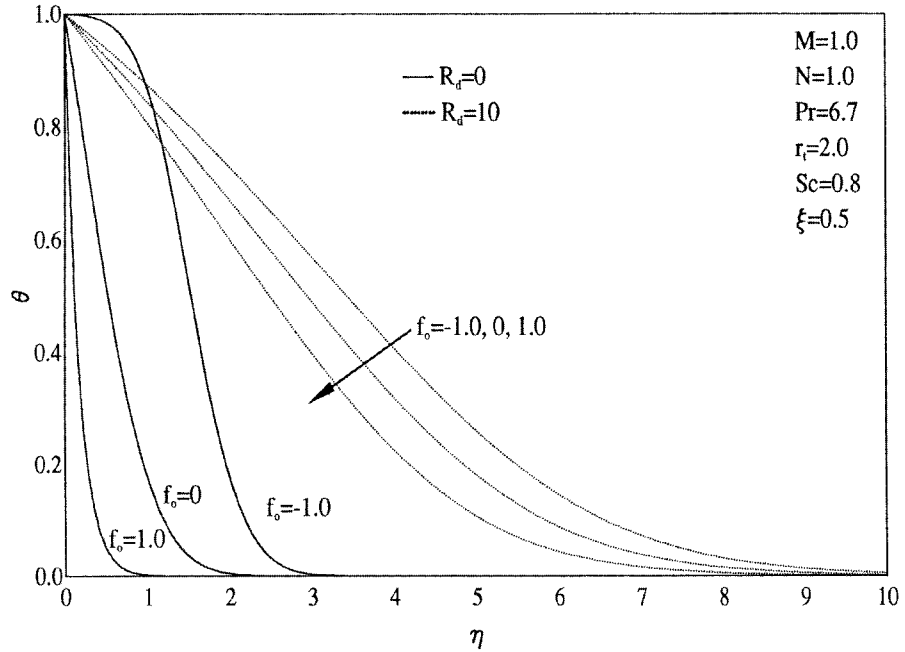

Figure 15. Effects of f_o and R_d on temperature profiles.

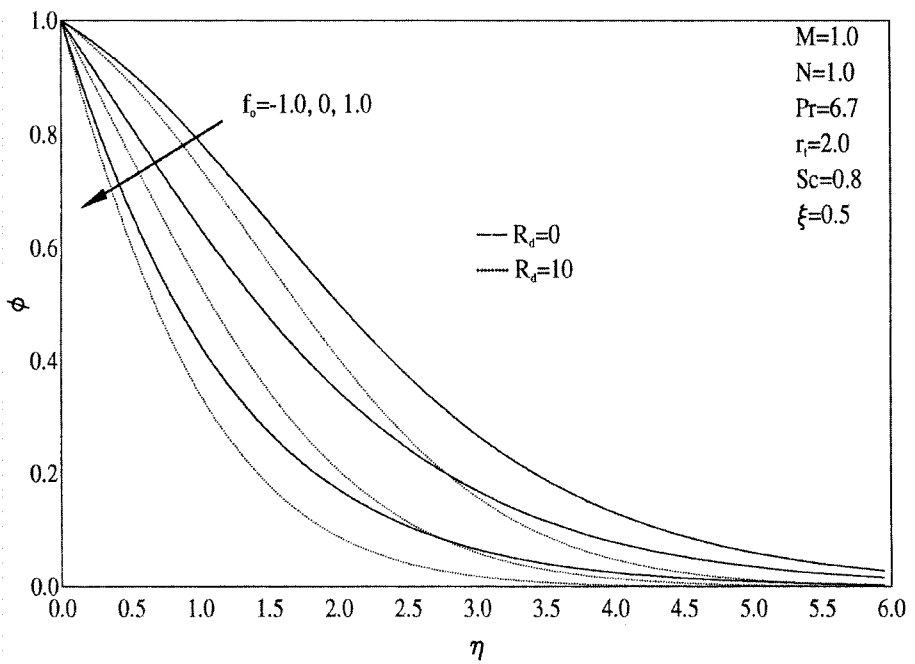

Figure 16. Effects of f_o and R_d on concentration profiles.

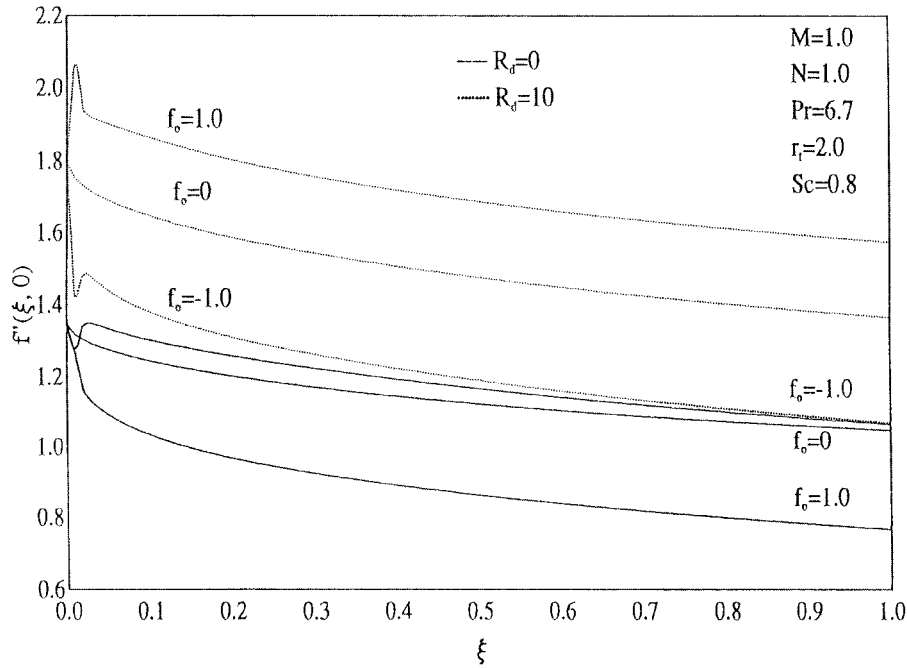

Figure 17. Effects of f_o and R_d on development of skin-friction coefficient.

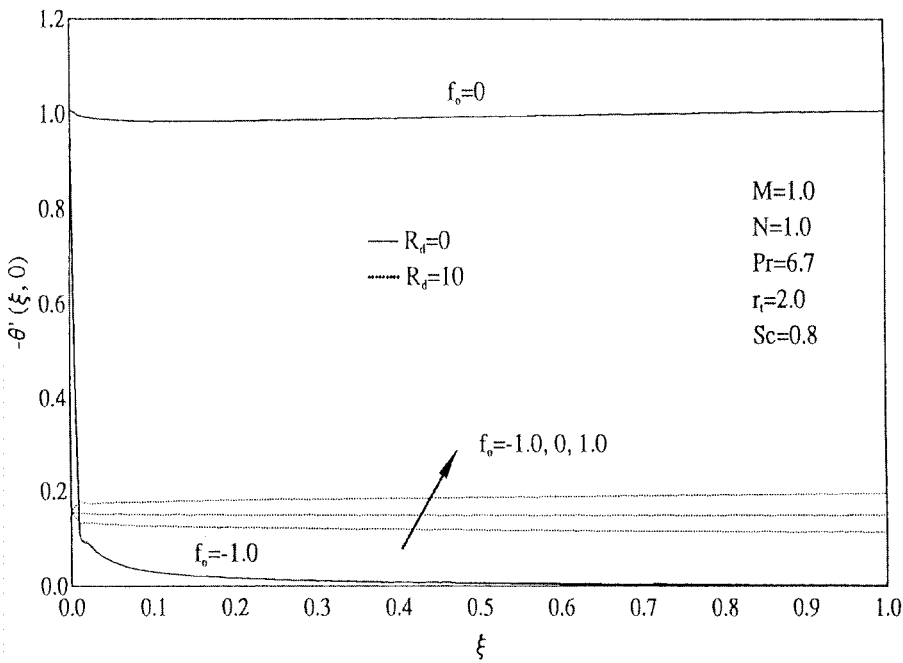

Figure 18. Effects of f_o and R_d on development of Nusselt numbers.

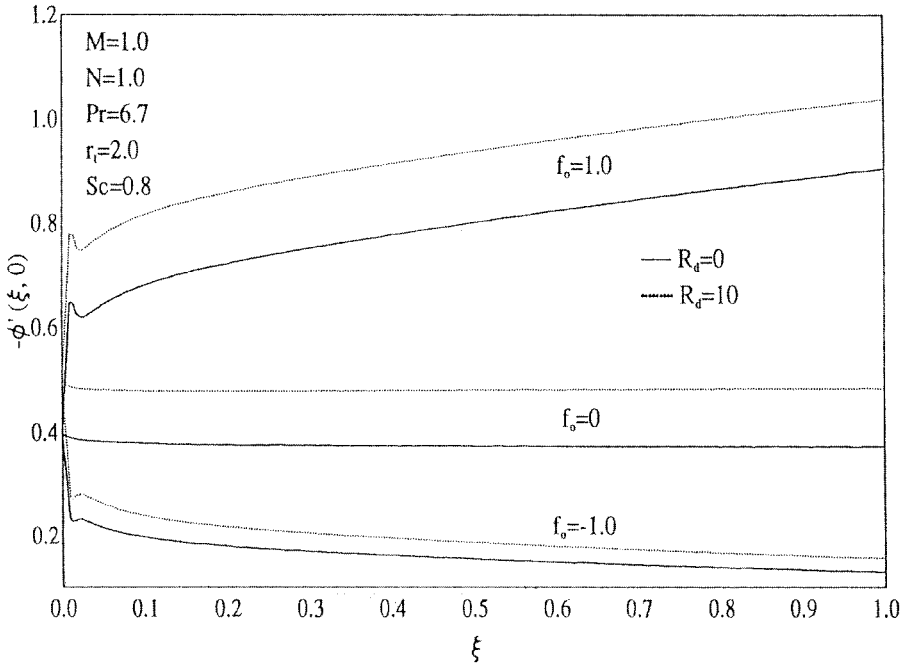

Figure 19. Effects of f_o and R_d on development of Sherwood number.

Inspection of the velocity, temperature, and concentration profiles reported in Figures 14 through 16 reveals that $(f''(0.5, 0))$ decreases for $R_d = 0$ and increases for $R_d = 10$ as f_o increases and $(f''(0.5, 0))$ is higher for $R_d = 10$ than that of $R_d = 0$. The same behavior apparently exists for other values of ξ with small overshoots and undershoots close to $\xi = 0$ and then a continuously decaying trend with ξ. It also reveals that $-\phi'(0.5, 0)$ increases as either of f_o or R_d increases and that $-\phi'(\xi, 0)$ has a decaying trend with ξ for $f_o < 0$, an increasing behavior with ξ for $f_o > 0$, whereas it remains almost constant with ξ for $f_o = 0$. The behavior of $-\theta'(\xi, 0)$ is, however, somewhat different for $R_d = 0$ where it decreases and increases sharply with ξ for $f_o < 0$ and $f_o > 0$, respectively while it remains almost constant for $f_o = 0$. The curve associated with $f_o = 1.0$ (for $R_d = 0$) lies outside the range of the figure and, therefore, is not shown. In addition, while for $R_d = 10$ the values of $-\theta'(\xi, 0)$ are lower than those corresponding to $R_d = 0$ for $f_o \geq 0$, they are higher for $f_o < 0$ than those corresponding to $R_d = 0$ except at very small values of ξ. It should be mentioned that the behavior of the local Nusselt number will be different than given in Figure 18 for $R_d = 10$ (as evident from Eqs. (15)) where its values will be higher than those associated with $R_d = 0$ for all values of f_o. All of the above trends are evident from Figures 17 through 19.

Finally, Table 3 reports values for $f''(\infty, 0)$, $-\theta'(\infty, 0)$, and $-\phi'(\infty, 0)$ for various values of M and N. Again, it is seen that as M increases all of $f''(\infty, 0)$, $-\theta'(\infty, 0)$, and $-\phi'(\infty, 0)$ decrease. However, the opposite effect is predicted where all of these physical parameters increase as N increases.

Table 3 Values of $f''(\infty, 0)$, $-\theta'(\infty, 0)$, and $-\phi'(\infty, 0)$ for various values of M and N with $f_o = 0$, $\Pr = 6.7$, $r_t = 2.0$, $R_d = 10$, $\mathrm{Sc} = 0.8$

M	N	$f''(\infty, 0)$	$-\theta'(\infty, 0)$	$-\phi'(\infty, 0)$
0	0	1.56320	0.20074	0.63531
1	0	0.11021	0.02301	0.05908
2	0	0.05519	0.02026	0.03699
0	−1	0.00010	0.01200	0.02602
0	0	0.07997	0.02325	0.06384
0	3	0.31810	0.03043	0.11483

CONCLUSION

The problem of steady-state, laminar heat and mass transfer by natural convection boundary layer flow around a permeable truncated cone in the presence of magnetic field and thermal radiation effects was considered. A set of nonsimilar governing differential equations was obtained and solved numerically by an implicit finite difference methodology. Comparisons with previously published work on various special cases of the general problem were performed and the results were found to be in excellent agreement. A representative set of numerical results for the velocity, temperature, and concentration profiles as well as the local skin-friction coefficient, local Nusselt number, and the local Sherwood number was presented graphically and discussed. It was found that, in general, all of the local skin-friction coefficients, local Nusselt number, and the local Sherwood number reduced as the magnetic Hartmann number was increased. Also, while all of these physical parameters decreased with the distance along the cone surface in the presence of the magnetic field, they increased with it in the absence of the magnetic field. It was also found that owing the presence of flow-aiding concentration buoyancy effects, all of the local skin-friction coefficient, local Nusselt number, and the local Sherwood number increased. The effects of fluid suction at the cone surface was found to decrease the local skin-friction coefficient in the absence of thermal radiation effects and to increase it when the radiation effects were present. However, both the local Nusselt and Sherwood numbers were found to increase as the suction velocity was increased regardless of the presence or absence of thermal radiation effects.

REFERENCES

1. T. K. Aldoss, M. A. Al-Nimr, M. A. Jarrah, and B. J. Al-Sha'er, Magnetohydrodynamic Mixed Convection from a Vertical Plate Embedded in a Porous Medium, *Numer. Heat Transfer, A*, vol. 28, pp. 635–645, 1995.
2. T. T. Kao, Local Nonsimilar Solution for Laminar Free Convection Adjacent to a Vertical Wall, *Transactions of ASME Journal of Heat Transfer*, vol. 98, pp. 321–322, 1976.
3. T. Y. Na, Numerical Solution of Natural Convection Flow Past a Non-Isothermal Vertical Flat Plate, *Applied Scientific Research*, vol. 33, pp. 519–543, 1978.

4. H. T. Lin and C. C. Chen, Mixed Convection on Vertical Plate for Fluids of Any Prandtl Number, *Warme-und Stoffubertragung*, vol. 22, pp. 159–168, 1988.
5. R. G. Hering and R. J. Grosh, Laminar Free Convection from a Non-Isothermal Cone at Low Prandtl Number, *Int. J. Heat Mass Transfer*, vol. 8, pp. 1333–1337, 1965.
6. S. Roy, Free Convection from a Vertical Cone at High Prandtl Numbers, *Transactions of ASME Journal of Heat Transfer*, vol. 96, pp. 115–117, 1974.
7. M. Alamgir, Over-all Heat Transfer from Vertical Cones in Laminar Free Convection: An Approximate Method, *Transactions of ASME Journal of Heat Transfer*, vol. 101, pp. 174–176, 1979.
8. T. Y. Na and J. P. Chiou, Laminar Natural Convection over a Slender Vertical Frustum of a Cone, *Warme-und Stoffubertragung*, vol. 12, pp. 83–87, 1979.
9. T. Y. Na and J. P. Chiou, Laminar Natural Convection over a frustum of a Cone, *Applied Scientific Research*, vol. 35, pp. 409–421, 1979.
10. N. G. Kafoussias, MHD Free Convection Flow through a Nonhomogeneous Porous Medium over an isothermal Cone Surface, *Mech. Res. Commun.*, vol. 19, pp. 89–94, 1992.
11. M. Kumari, H. S. Takhar, and G. Nath, Nonaxisymmetric Unsteady Motion over a Rotating Disk in the Presence of Free Convection and Magnetic Field, *Int. J. Engng. Sci.*, vol. 31, pp. 1659–1668, 1993.
12. A. Raptis and A. K. Singh, MHD Free Convection Flow Past an Accelerated Vertical Plate, *Int. Commun. Heat Mass Transfer*, vol. 10, pp. 313-321, 1983.
13. H. S. Takhar and P. C. Ram, Magnetohydrodynamics Free Convection Flow of Water at 4°C, through a Porous Medium, *Int. Commun. Heat Mass Transfer*, vol. 21, pp. 371–376, 1994.
14. R. Viskanta and R. J. Grosh, Boundary Layer in Thermal Radiation Absorbing and Emitting Media, *Int. J. Heat Mass Transfer*, vol. 5, pp. 795–806, 1962.
15. M. M. Ali, T. S. Chen, and B. F. Armaly, Natural Convection-Radiation Interaction in Boundary-Layer Flow over Horizontal Surfaces, *AIAA Journal*, vol. 22, pp. 1797–1803, 1984.
16. M. A. Hossain and M. A. Alim, Natural Convection-Radiation Interaction on Boundary Layer Flow along a Thin Vertical Cylinder, *Heat Mass Transfer*, vol. 32, pp. 515–520, 1997.
17. M. A. Hossain and D. A. S. Rees, Free Convection-Radiation Interaction from an Isothermal Plate Inclined at a small Angle to the Horizontal, *Acta Mechanica*, vol. 127, pp. 63–73, 1998.
18. M. A. Hossain, M. A. Alim, and D. A. S. Rees, Effect of Thermal Radiation on Natural Convection over Cylinders of Elliptic Cross Section, *Acta Mechanica*, vol. 129, pp. 177–186, 1998.
19. K. A. Yih, Effect of Radiation on Natural Convection about a Truncated Cone, *Int. J. Heat Mass Transfer*, vol. 42, pp. 4299–4305, 1999.
20. F. G. Blottner, Finite-Difference Methods of Solution of the Boundary-Layer Equations, *AIAA J.*, vol. 8, pp. 193–205, 1970.
21. T. Cebeci and P. Bradshaw, *Physical and Computational Aspects of Convective Heat Transfer*, 1st ed. Springer, New York, p. 270, 1984.
22. W. M. Kays and M. E. Crawford, *Convective Heat and Mass Transfer*, 3rd ed. McGraw-Hill, New York, p. 402, 1980.